

Edinburgh Preprint: 92/507

Liverpool Preprint: LTH 301

Southampton Preprint: SHEP 92/93-13

hep-lat/9307009

Revised 30 June 1993

# Quenched Light Hadron Mass Spectrum and Decay Constants: the effects of $O(a)$ -Improvement at $\beta = 6.2$

*UKQCD Collaboration*

**C.R. Allton<sup>1</sup>, C.T. Sachrajda**

Physics Department, The University, Southampton SO9 5NH, UK

**R.M. Baxter, S.P. Booth, K.C. Bowler, S. Collins, D.S. Henty, R.D. Kenway,  
C. McNeile<sup>2</sup>, B.J. Pendleton, D.G. Richards, J.N. Simone, A.D. Simpson**  
Department of Physics, The University of Edinburgh, Edinburgh EH9 3JZ, Scotland

**A. McKerrell, C. Michael, M. Prisznyak,**  
DAMTP, University of Liverpool, Liverpool L69 3BX, UK

## Abstract

We compare the light hadron spectrum and decay constants for quenched QCD at  $\beta = 6.2$  using an  $O(a)$ -improved nearest-neighbour Wilson fermion action with those obtained using the standard Wilson fermion action on the same set of 18 gauge configurations. For pseudoscalar meson masses in the range 330–800 MeV, we find no significant difference between the results for the two actions. The scales obtained from the string tension and mesonic sector are consistent, but differ from that derived from baryon masses. The ratio of the pseudoscalar decay constant to the vector meson mass increases slowly with quark mass as observed experimentally.

---

<sup>1</sup>Present address: Dipartimento di Fisica, Università di Roma *La Sapienza*, 00185 Roma, Italy

<sup>2</sup>Present address: Dept. of Physics & Astronomy, University of Kentucky, Lexington KY 40506, USA

# 1 Introduction

The numerical simulation of QCD involves systematic errors arising from a variety of sources: non-zero lattice spacing, finite volume, quenching and/or unphysical quark masses. Here we address the first of these by working in the quenched approximation at a fixed volume, and comparing the results obtained on the same set of gauge configurations using two formulations of the fermion action with different discretisation errors.

Classically, the standard Wilson pure gauge action differs from the continuum Yang-Mills action by terms of  $O(a^2)$ , where  $a$  is the lattice spacing [1], whereas the Wilson formulation of lattice fermions introduces an  $O(a)$  discretisation error in order to avoid the doubling problem. At the quantum level, matrix elements computed with the Wilson action have errors of  $O(a)$ . Monte-Carlo determinations of the renormalisation constants of the vector current have shown that these discretisation errors may be as large as 30% [2].

In the spirit of the Symanzik improvement programme [3], which sought to eliminate in a systematic way discretisation errors at the quantum level, Wetzel [4] proposed a two-link fermion action which cancels the  $O(a)$  term in the Wilson action at tree level. In a study of on-shell improvement, Sheikholeslami and Wohlert [5] introduced a nearest-neighbour  $O(a)$ -improved fermionic action, which is more convenient for large scale simulations and which we refer to as the ‘SW’ action. This may be obtained from the two-link action by a rotation of fermion fields in the functional integral. Heatlie et al. [2] demonstrated the absence of the leading logarithmic terms at  $n^{\text{th}}$  order in perturbation theory, in matrix elements of rotated operators. These terms are of the form  $g_0^{2n} a \ln^n a$ , and hence effectively  $O(a)$  in the weak coupling regime, because  $g_0^2 \sim 1/\ln a$ .

In this paper we present further details of a study in quenched QCD on a  $24^3 \times 48$  lattice at  $\beta = 6.2$ , using both the standard  $r = 1$  Wilson fermion action:

$$S_F^W = \sum_x \left\{ \bar{q}(x)q(x) - \kappa \sum_\mu \left[ \bar{q}(x)(1 - \gamma_\mu)U_\mu(x)q(x + \hat{\mu}) + \bar{q}(x + \hat{\mu})(1 + \gamma_\mu)U_\mu^\dagger(x)q(x) \right] \right\} \quad (1)$$

and the SW fermion action [5]:

$$S_F^{SW} = S_F^W - i \frac{\kappa}{2} \sum_{x,\mu,\nu} \bar{q}(x)F_{\mu\nu}(x)\sigma_{\mu\nu}q(x). \quad (2)$$

$F_{\mu\nu}$  is a lattice definition of the field strength tensor, which we take to be the sum of the four untraced plaquettes in the  $\mu\nu$  plane open at the point  $x$  [5], as indicated in Figure 1:

$$F_{\mu\nu}(x) = \frac{1}{4} \sum_{\square=1}^4 \frac{1}{2i} \left[ U_{\square\mu\nu}(x) - U_{\square\mu\nu}^\dagger(x) \right]. \quad (3)$$

For this reason, the SW action is sometimes called the ‘clover’ action [6].

Our objective is to look for evidence of improvement in masses and decay constants of the light hadrons. A summary of our results has appeared in [6], where we concluded that the

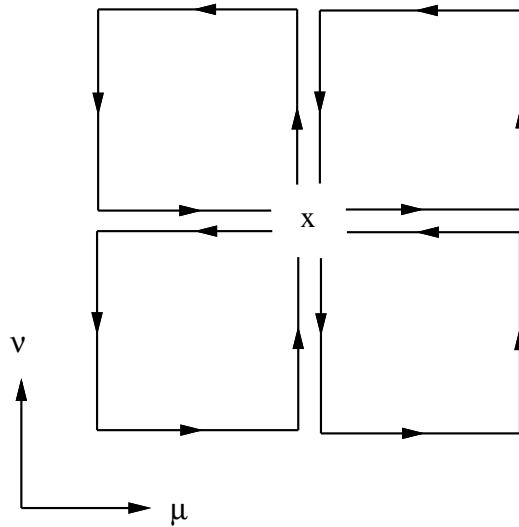


Figure 1: Lattice definition of the field strength tensor,  $F_{\mu\nu}(x)$ .

SW action for medium to light quark masses gives results in agreement with the Wilson action, although typically with a noisier signal. In this paper, we report our attempts to enhance the signal when using the SW action by smearing the same set of propagators at the sink.

The plan of the paper is as follows. We begin by describing the generation of the gauge fields, and the measurement of the static quark-antiquark potential used to extract the lattice spacing in physical units from the string tension. We describe the algorithms used to compute the quark propagators, and the bootstrap method used to analyse the hadron correlators. We compare the meson and baryon spectra for the two actions, and extract values for the lattice spacing by comparing the masses to their physical values. We investigate the hyperfine mass splittings as quantities that might be sensitive to the difference between the actions. Finally, we compute the pseudoscalar and vector meson decay constants.

## 2 Computational Procedure

The gauge field configurations and quark propagators were obtained using the Meiko i860 Computing Surface at Edinburgh. This is a MIMD system of 64 nodes, each of which consists of one Intel i860 processor on which the application runs, two Inmos T800's for inter-node communications and 16 MBytes of memory. The peak performance is 5 Gflops in 32-bit arithmetic. Our codes are written in ANSI C with key numerically-intensive routines in i860 assembler, and communications using Meiko CS-Tools [7, 8]. Apart from certain global operations which use 64 bits, the calculations are performed in 32-bit arithmetic. We achieve

a maximum performance of 3 Gflops for some routines, while overall our programs sustain around 1.5 Gflops [9].

## 2.1 Gauge Configurations

### 2.1.1 Update algorithm

There are computational advantages in using an over-relaxation (OR) algorithm for updating, both from the speed of the code itself and from the improved transport through the space of equilibrium configurations. For  $SU(2)$  pure gauge theory, such an algorithm is very simple and hence computationally fast. For  $SU(3)$  pure gauge theory, there is no such simple implementation known. The proposal of Creutz [10] uses an approximate over-relaxation which has to be corrected by an accept/reject calculation. Furthermore, a projection of a  $3 \times 3$  complex matrix to  $SU(3)$  is needed, which is computationally slow.

As an alternative, we explored the possibility of using OR steps in a sequence of  $SU(2)$  subgroups of  $SU(3)$ . This is in the spirit of the Cabibbo-Marinari [11] scheme of updating  $SU(3)$  via  $SU(2)$  subgroups. Our  $SU(2)$  subgroup OR scheme is exactly micro-canonical, unlike the Creutz scheme. In order to optimise this  $SU(2)$  subgroup OR approach, we measured the average distance moved by a link in the  $SU(3)$  group manifold (along a geodesic) for different subgroup updating schemes. Using 3 subgroups (12, 23 then 31) was optimal and gave a distance moved slightly less than the Creutz scheme, but significantly more than the Cabibbo-Marinari heat-bath update. A check of auto-correlation between configurations was made and confirmed that this  $SU(2)$  OR scheme is competitive. Because of its computational speed, we chose to use this 3 subgroup  $SU(2)$  OR algorithm, complemented by one heat-bath update every 5 OR updates to preserve ergodicity. We call this type of algorithm ‘Hybrid Over-Relaxed’. At the end of each  $5 + 1$  sweeps, we re-unitarise each element of the gauge configuration by normalising the first row of the  $SU(3)$  matrix, making the second row orthonormal to the first and then reconstructing the third row from the appropriate vector product. We have checked that any systematic effect arising from this procedure is negligible.

Whenever the gauge configuration is written to disk, the last operation performed on it is a re-unitarisation. This allows us to write only the first two rows of each matrix and yet re-start from the identical configuration by reconstructing the final row.

Random numbers were generated using the *uni* random number generator [12]. Each processor used a separate copy of the generator, initialised with different starting states.

The results presented here are based on an analysis for each action of the same set of 18 configurations, starting at configuration 16800 and separated by 2400 sweeps.

### 2.1.2 Static quark–antiquark potential

The potential between static colour sources at separation  $R$  can be obtained by measuring Wilson loops of size  $R \times T$ . However, it is useful to consider generalised correlations of size  $R \times T$  where the spatial paths are any gauge invariant path with cylindrical symmetry ( $A_{1g}$ ), not just the straight line used in a rectangular Wilson loop. Moreover, the two spatial paths, at times  $T$  apart, may be different. So the measurable is  $C_{ij}(R, T)$  where  $i, j$  label the path type. Then the largest eigenvalue,  $\lambda(R)$ , of the transfer matrix in the presence of the static sources is related to the potential by

$$V(R) = -\log(\lambda(R)) \quad (4)$$

and  $\lambda(R)$  can be obtained from the limit as  $T \rightarrow \infty$  of the largest eigenvalue,  $\lambda(R, T)$ , of the equation

$$C_{ij}(R, T)u_j = \lambda(R, T)C_{ij}(R, T - 1)u_j. \quad (5)$$

This is a variational method where an optimal combination of paths  $i$  (with  $i = 1, \dots, N$ ) is chosen. The best choice of paths would allow  $\lambda(R, T)$  to be close to its asymptotic value for small  $T$ . In this way the statistical errors are minimised. Thus it is convenient to introduce an ‘overlap’ defined as

$$\mathcal{O}(R) = \prod_T \{\lambda(R, T)/\lambda(R)\}. \quad (6)$$

For  $R = 12$  straight paths, we find  $\mathcal{O} < 0.006$ . Thus rectangular Wilson loops are a very inaccurate way of extracting the ground state potential.

As has been known for some time, an efficient improvement comes from fuzzing or blocking these paths [13, 14, 15]. Using a purely spatial blocking allows the transfer matrix interpretation to be retained. Because of its flexibility, we used the recursive blocking scheme [14]:

$$U(\text{new}) = \mathcal{P}_{SU(3)} \left[ cU(\text{straight}) + \sum_1^4 U(\text{u-bends}) \right]. \quad (7)$$

After exploratory studies to optimise the overlap  $\mathcal{O}$ , we chose  $c = 4$  and a maximum of 40 iterations of this recursive blocking. As a variational basis with  $N = 2$ , we used 40 and 28 iterations for the paths. This basis for  $R = 12$  yields an overlap  $\mathcal{O} = 0.95$  which is a huge improvement over the purely unblocked case. Because this value of the overlap is close to 1.0, one can get reliable estimates of the ground state potential from quite small  $T$ -values such as  $T = 3$ . A powerful cross check of this extraction of the ground state energy at rather small  $T$ -values comes from determining the first excited state also in the variational method. From previous work, this first excited  $A_{1g}$  potential should lie about  $2\pi/R$  higher [15] and this is completely consistent with our results.

To estimate the potential  $V(R)$ , we need to extrapolate in  $T$ . For  $1 \leq R \leq 4$ , we find that the 3 : 2 and 4 : 3  $T$ -ratio results for  $\lambda(R, T)$  are consistent within errors. As a conservative

$R$	$V(R)$	$V(R+1) - V(R)$
1	0.3775(2)	0.1564(3)
2	0.5339(3)	0.0787(5)
3	0.6126(7)	0.0509(5)
4	0.6635(8)	0.0416(12)
5	0.7043(17)	0.0348(14)
6	0.7392(26)	0.0316(19)
7	0.7707(27)	0.0300(19)
8	0.8008(39)	0.0304(24)
9	0.8311(37)	0.0295(23)
10	0.8606(53)	0.0212(29)
11	0.8819(60)	0.0322(26)
12	0.9140(60)	

Table 1: The potential and force at  $\beta = 6.2$ .

estimate of the asymptotic value we used the 4 : 3  $T$ -ratio to evaluate  $V(R)$ . For  $R \geq 5$ , we find a small but statistically significant difference between the 3 : 2 and 4 : 3  $T$ -ratio results. This we extrapolate to large  $T$  using the estimate of the first excited state energy referred to above. Statistical errors come from a bootstrap analysis of the variation over our 18 sample configurations, where the variational path combination is fixed by the 1 : 0  $T$ -ratio analysis. This avoids the possibility that the variational approach is influenced by the statistical error. Results are shown in Table 1.

We also fit the static potential for  $R \geq 2$  with a lattice Coulomb plus linear term:

$$V(R) = C - \frac{E}{R_L} + KR \quad (8)$$

where  $1/R_L$  is the discrete Coulomb Green function. Using a fit to the previously determined values of  $V(R)$  and taking into account correlations in errors between potentials at different  $R$ -values, we find the result of Table 2. Here the error quoted is statistical; it includes the error from the data sample variation and the  $T$ -extrapolation described above, but not the systematic effect of using different fit functions. This value for the string tension enables us to set the scale by requiring  $a^{-1}\sqrt{K} = 0.44$  GeV, so yielding  $a^{-1} = 2.73(5)$  GeV. This implies that the potential has been measured to a physical distance,  $Ra$ , of 0.87 fermi. Using the conventional 2-loop perturbative relationship between  $\Lambda$  and  $a$  yields  $\sqrt{K}/a\Lambda_L \leq 85.9(1.5)$ , where the inequality arises because of the observed lack of asymptotic scaling at  $\beta = 6.2$ .

These results are in agreement with a similar analysis on  $20^4$  lattices at the same  $\beta$ -value [15, 16]. This confirms the conclusion of that work that finite-size effects are small for the

$E$	$K$
0.274(6)	0.0259(9)

Table 2: Fit to the force for  $R > 1$ .

potential on lattices with  $L \geq 20$ . A recent independent analysis on a  $24^3 \times 32$  lattice [17] gives a result for the string tension which also agrees with ours. From a comparison of our result for the string tension with those at neighbouring  $\beta$  values, we find that asymptotic scaling is not obeyed. This can be understood because the lattice bare coupling is a poor expansion parameter [18]. The study of large lattices at larger  $\beta$  confirms this [19] and shows that the use of a more physical coupling gives excellent agreement with perturbation theory to two loops, allowing  $\Lambda$  to be related to the string tension.

## 2.2 Quark Propagators

To calculate the quark propagator we need to solve equations of the form

$$(\mathcal{A} - \kappa\mathcal{B})G(x, 0) = \eta_{x,0}. \quad (9)$$

where, for either action,  $\mathcal{A}$  is purely local and  $\mathcal{B}$  connects only nearest-neighbour sites. We have investigated the least residual (LR) and least norm (LN) variants [20] of the Conjugate Gradient (CG) algorithm, and an Over-Relaxed Minimal Residual (MR) algorithm [21, 22]. We also implemented a simple preconditioning which involves left-multiplying Equation (9) by  $(1 + \kappa\mathcal{B}\mathcal{A}^{-1})$ . This decouples even and odd lattice sites so that Equation (9) becomes

$$(\mathcal{A} - \kappa^2\mathcal{B}\mathcal{A}^{-1}\mathcal{B})G^{\text{even}} = \eta^{\text{even}} + \kappa\mathcal{B}\mathcal{A}^{-1}\eta^{\text{odd}} \quad (10)$$

$$G^{\text{odd}} = \mathcal{A}^{-1}\eta^{\text{odd}} + \kappa\mathcal{A}^{-1}\mathcal{B}G^{\text{even}}. \quad (11)$$

We solve Equation (10) for  $G^{\text{even}}$  and substitute into Equation (11) to obtain  $G^{\text{odd}}$ . For all the algorithms and for both actions, we found that this red-black preconditioning gave a factor of between 2.5 and 3.0 decrease in the number of iterations required, without increasing significantly the number of floating-point operations per iteration.

Writing

$$\mathcal{M} = \mathcal{A} - \kappa^2\mathcal{B}\mathcal{A}^{-1}\mathcal{B} \quad (12)$$

$$\zeta = \eta^{\text{even}} + \kappa\mathcal{B}\mathcal{A}^{-1}\eta^{\text{odd}} \quad (13)$$

the MR algorithm is

$$r_0 = \zeta - \mathcal{M}G_0^{\text{even}}$$

repeat until convergence

$$\alpha = \frac{(\mathcal{M}r_i, r_i)}{(\mathcal{M}r_i, \mathcal{M}r_i)}$$

$$\alpha' = \Omega\alpha \quad (\text{over-relaxation})$$

$$G_{i+1}^{\text{even}} = G_i^{\text{even}} + \alpha' r_i$$

$$r_{i+1} = r_i - \alpha' \mathcal{M}r_i.$$

We found that choosing the over-relaxation parameter,  $\Omega$ , to be 1.1 gave a gain from over-relaxation of a few per cent. This is in agreement with the data in [21], which indicates that the gains from over-relaxation decrease as  $\beta$  increases. However, for both actions and throughout the physical regime investigated, MR typically converges to a solution in fewer iterations than CG, with each iteration taking about half the time. Therefore, we always use an over-relaxed MR algorithm with red-black preconditioning.

In order to obtain an improved matrix element of an operator containing quark fields, in addition to using the SW action, the quark fields must be rotated according to [2, 23]:

$$q \rightarrow q' = \left(1 - \frac{1}{2}\gamma \cdot \vec{D}\right) q \quad (14)$$

$$\bar{q} \rightarrow \bar{q}' = \bar{q} \left(1 + \frac{1}{2}\gamma \cdot \overleftarrow{D}\right) \quad (15)$$

where we have used the equation of motion for the quark fields to remove the bare mass from the rotation. The lattice covariant derivatives are defined as follows:

$$\vec{D}_\mu f(x) = \frac{1}{2} \left( U_\mu(x) f(x + \hat{\mu}) - U_\mu^\dagger(x - \hat{\mu}) f(x - \hat{\mu}) \right) \quad (16)$$

and

$$f(x) \overleftarrow{D}_\mu = \frac{1}{2} \left( f(x + \hat{\mu}) U_\mu^\dagger(x) - f(x - \hat{\mu}) U_\mu(x - \hat{\mu}) \right). \quad (17)$$

We can define the rotated SW propagator,  $G^R(x, y)$ , by [24]

$$G^R(x, y) \equiv \left(1 - \frac{1}{2}\gamma \cdot \vec{D}\right) G(x, y) \left(1 + \frac{1}{2}\gamma \cdot \overleftarrow{D}\right). \quad (18)$$

This propagator includes the rotations (14) and (15) and so the evaluation of all correlation functions is performed in the same way as with the unimproved action; no further rotations of the operators are necessary. The evaluation of the rotated propagator,  $G^R$ , is only marginally more complicated than that of  $G$ ; solve the equation:

$$(\mathcal{A} - \kappa\mathcal{B})G'(x, y) = \eta_{x,y} + \frac{1}{2}\eta_{x,y}\gamma \cdot \overleftarrow{D} \quad (19)$$

then  $G^R$  is obtained easily from  $G'$  by

$$G^R(x, y) = \left(1 - \frac{1}{2}\gamma \cdot \vec{D}\right) G'(x, y). \quad (20)$$



Recently, there has been increasing evidence that lattice measurements can be enhanced through the use of non-local, or smeared operators [16, 25, 26]. The original attempts to use smeared operators for fermions are described in references [27, 28]. For propagator calculations, we can use a source,  $\eta$ , in Equation (9), which is extended over some non-zero spatial volume, called source smearing, or we can smear the solution, called sink smearing. Güsken et al. [25] have proposed a gauge-invariant smearing method based upon using the solution of the three-dimensional Klein-Gordon equation:

$$(1 - \kappa_S \mathbf{D}^2)\eta_{x,0} = \delta_{x,0} \quad (21)$$

for the source in Equation (9), where  $\mathbf{D}^2$  is the three-dimensional operator

$$\mathbf{D}^2 f(x) = \sum_{j=1}^3 \left( U_j(x) f(x + \hat{j}) + U_j^\dagger(x - \hat{j}) f(x - \hat{j}) \right). \quad (22)$$

Alternatively, sink smearing corresponds to solving

$$(1 - \kappa_S \mathbf{D}^2)G_{SL} = G^R \quad (23)$$

where  $G^R$  is the solution of Equation (20). The extent of the smearing is controlled by the single parameter,  $\kappa_S$ .

We label propagators with a local source and sink, LL, those with a local source but smeared sink, SL, and those with a smeared source but local sink, LS. In practice, we smear at the sink, as this has the advantage that the smearing can be undone with a single multiplication by  $(1 - \kappa_S \mathbf{D}^2)$ . Since we can thus easily recover the LL propagator from the SL propagator, we only write out the SL propagator to disk, a very significant advantage for our particular machine architecture. Details of our investigations of the effects of smearing are reported elsewhere [29].

We have calculated LL propagators at  $\kappa = 0.1510, 0.1520, 0.1523, 0.1526$  and  $0.1529$  for the Wilson action, LL and SL propagators at  $\kappa = 0.14144, 0.14226, 0.14244, 0.14262$  and  $0.14280$  for the SW action; the latter values were chosen to match roughly the pseudoscalar meson masses computed in the Wilson case. The boundary conditions used were periodic in space and antiperiodic in time. The scalar hopping parameter,  $\kappa_S$ , used in the computation of the SL SW propagators, was taken to be  $0.180$ , corresponding to a smearing radius [29] of approximately 2. The extra computational cost involved in using the SW action is difficult to quantify, being machine dependent. For the red-black preconditioned MR algorithm which we employed, each iteration took roughly 35% longer than for the Wilson action, but taking into account other fixed overheads, most notably I/O, the total elapsed time for a propagator calculation at a given pion mass was between 10% and 20% longer, whilst the memory requirement was some 10% more than in the Wilson case.

## 2.3 Analysis of 2-Point Functions

We obtain the amplitudes and masses of mesons (baryons) by correlated least- $\chi^2$  fits of a single cosh (exponential) function simultaneously to the appropriate forward and backward propagators. We require that the fitting region,  $[t_{\min}, t_{\max}]$ , satisfies the condition that, within the small range allowed by our statistics, changing  $t_{\min}$  gives the same mass within errors, while  $t_{\max}$  is taken as large as the growing noise/signal ratio allows. We find that the intervals  $[12, 16]$  for local sinks and  $[9, 13]$  for smeared sinks are satisfactory in this regard. The correlated  $\chi^2/\text{dof}$  varies between 0.3 and 4, which indicates both that we are taking correlations into account and that we are getting reasonable fits.

The covariance matrix is estimated using a single-removal jackknife. For simple averages, such as the propagator, this is the same as the data covariance matrix. We calculate the jackknife covariance matrix for the timeslices used in the fit. We employ a singular value decomposition in the construction of our matrix inverses, to detect singular or nearly singular matrices. Because of our limited statistics, we use timeslices 12, 14, 16, 32, 34 and 36 for local sinks, and 9, 11, 13, 35, 37 and 39 for smeared sinks. We currently have too few configurations to deal with the  $\kappa - \kappa$  correlations directly in the fits. Therefore we do individual fits for each  $\kappa$  value. We recover the effect of the  $\kappa$  correlations in our analysis of the errors.

To estimate our errors, we use the bootstrap resampling method, a concise description of which has been given by Chu et al. [30]. From our set of 18 Monte Carlo samples of the probability distribution for the link variables, we construct a bootstrap sample by drawing 18 configurations independently and with replacement. We perform exactly the same analysis on this sample of 18 configurations as on the original set, to obtain a bootstrap estimate of average quantities. We then build up the bootstrap distribution by drawing 1000 bootstrap samples with corresponding bootstrap estimates of averages. We reconstruct the covariance matrix for each bootstrap sample so as to take into account the uncertainty in the covariance matrix. We then bin the bootstrap determinations of the average to determine confidence limits. The quoted errors are obtained by requiring that the central 68% of the bootstrap values lie within the error bars.

For every quantity fitted, we use the same sequence of bootstrap samples and store the best fit to the original set, together with the bootstrap determinations. Thus the  $i$ 'th bootstrap estimate of any quantity, is the result of a fit to the  $i$ 'th sample of 18 configurations. In this way we preserve information on correlations between physical quantities at, say, different  $\kappa$  values.

## 3 Hadron Spectrum

### 3.1 Masses and Matrix Elements

We present results for the pseudoscalar meson (P), vector meson (V), nucleon (N) and  $\Delta$  using the following local interpolating fields:

$$P = \bar{u}\gamma_5 d \quad (24)$$

$$V_i = \bar{u}\gamma_i d \quad (25)$$

$$N = \epsilon_{abc}(u^a C\gamma_5 d^b)u^c \quad (26)$$

$$\Delta_\mu = \epsilon_{abc}(u^a C\gamma_\mu u^b)u^c. \quad (27)$$

For the vector meson, we average our correlators over the three polarisation states, for the nucleon we average the 11 and 22 spinor indices of the correlator, and for the  $\Delta$  we project out the spin-3/2 component and average over the four spin projections.

The mass estimates in lattice units obtained for the Wilson action using local sources and sinks are given in Table 3. Also included are the amplitudes,  $A$ , and  $\chi^2/\text{dof}$  obtained in the single cosh or exponential fits to the zero-momentum timeslice propagators:

$$\sum_{\mathbf{x}} \langle h(\mathbf{x}, t) h^\dagger(0) \rangle \sim \begin{cases} A_h (e^{-m_h t} + e^{-m_h(L_t-t)}), & \text{(mesons)} \\ A_h e^{-m_h t}, & t < L_t/2, \quad \text{(baryons)} \end{cases} \quad (28)$$

described above, where  $L_t = 48$  is the total time extent of our lattice. The corresponding results for the SW action using local sources with both local and smeared sinks are given in Table 4.

The Edinburgh plots for the LL data for both actions are given in [6]. That for the SW SL results is plotted in Figure 2. The plots are broadly consistent, showing a trend towards the experimental value for  $m_N/m_\rho$  with decreasing pseudoscalar meson mass. However, a comparison of the SW LL and SL plots reveals that the errors in the SL data are smaller than those of the LL data by at least 50%. This reduction is attributable to the better signal for the nucleon correlator using the SL data; comparing the results for the baryon masses at the lightest quark mass for LL and SL in Table 4, we note that the signal increases from approximately  $2\sigma$  to around  $4\sigma$  from zero. For this reason, we employ SL data, wherever possible, in making our comparisons of the SW and Wilson hadron masses.

### 3.2 Chiral Extrapolations

We now consider chiral extrapolation of the hadron masses in order to estimate the lattice scale for the two actions.

Wilson (LL)						
$\kappa$	0.1510	0.1520	0.1523	0.1526	0.1529	0.15328 <sup>+7</sup> <sub>-4</sub>
$m_P$	0.295 <sup>+6</sup> <sub>-3</sub>	0.221 <sup>+9</sup> <sub>-3</sub>	0.195 <sup>+9</sup> <sub>-3</sub>	0.164 <sup>+11</sup> <sub>-4</sub>	0.122 <sup>+9</sup> <sub>-11</sub>	0.0
$A_P \times 10^1$	0.121 <sup>+8</sup> <sub>-7</sub>	0.118 <sup>+9</sup> <sub>-7</sub>	0.124 <sup>+10</sup> <sub>-7</sub>	0.140 <sup>+15</sup> <sub>-10</sub>	0.180 <sup>+25</sup> <sub>-46</sub>	
$\chi^2/\text{dof}$	2.1/4	1.8/4	1.5/4	1.8/4	2.0/4	
$m_V$	0.377 <sup>+11</sup> <sub>-5</sub>	0.332 <sup>+15</sup> <sub>-4</sub>	0.321 <sup>+16</sup> <sub>-6</sub>	0.310 <sup>+19</sup> <sub>-11</sub>	0.298 <sup>+39</sup> <sub>-34</sub>	0.277 <sup>+25</sup> <sub>-9</sub>
$A_V \times 10^1$	0.130 <sup>+19</sup> <sub>-13</sub>	0.102 <sup>+19</sup> <sub>-7</sub>	0.095 <sup>+2</sup> <sub>-1</sub>	0.089 <sup>+2</sup> <sub>-1</sub>	0.086 <sup>+4</sup> <sub>-2</sub>	
$\chi^2/\text{dof}$	4.5/4	6.6/4	7.4/4	7.3/4	10.0/4	
$m_N$	0.591 <sup>+11</sup> <sub>-6</sub>	0.509 <sup>+15</sup> <sub>-7</sub>	0.480 <sup>+16</sup> <sub>-9</sub>	0.445 <sup>+16</sup> <sub>-13</sub>	0.395 <sup>+48</sup> <sub>-42</sub>	0.393 <sup>+20</sup> <sub>-16</sub>
$A_N \times 10^4$	0.217 <sup>+33</sup> <sub>-22</sub>	0.132 <sup>+32</sup> <sub>-16</sub>	0.109 <sup>+27</sup> <sub>-15</sub>	0.085 <sup>+24</sup> <sub>-15</sub>	0.062 <sup>+47</sup> <sub>-23</sub>	
$\chi^2/\text{dof}$	1.2/4	5.1/4	5.5/4	6.4/4	12.4/4	
$m_\Delta$	0.647 <sup>+19</sup> <sub>-10</sub>	0.582 <sup>+23</sup> <sub>-9</sub>	0.560 <sup>+23</sup> <sub>-11</sub>	0.538 <sup>+36</sup> <sub>-18</sub>	0.533 <sup>+116</sup> <sub>-40</sub>	0.496 <sup>+31</sup> <sub>-16</sub>
$A_\Delta \times 10^3$	0.109 <sup>+27</sup> <sub>-15</sub>	0.065 <sup>+19</sup> <sub>-9</sub>	0.051 <sup>+14</sup> <sub>-7</sub>	0.039 <sup>+20</sup> <sub>-8</sub>	0.039 <sup>+104</sup> <sub>-14</sub>	
$\chi^2/\text{dof}$	1.4/4	2.5/4	6.2/4	8.4/4	5.6/4	

Table 3: Hadron masses and amplitudes, in lattice units, for the Wilson action. The last column contains the values obtained by linear extrapolation to  $m_P = 0$ .

SW (LL)						
$\kappa$	0.14144	0.14226	0.14244	0.14262	0.14280	$0.14313^{+7}_{-4}$
$m_P$	$0.302^{+6}_{-4}$	$0.217^{+8}_{-6}$	$0.194^{+9}_{-6}$	$0.168^{+10}_{-6}$	$0.135^{+11}_{-6}$	0.0
$A_P \times 10^1$	$0.145^{+11}_{-12}$	$0.139^{+12}_{-14}$	$0.145^{+13}_{-15}$	$0.157^{+19}_{-17}$	$0.190^{+31}_{-25}$	
$\chi^2/\text{dof}$	3.0/4	1.8/4	1.4/4	1.4/4	2.5/4	
$m_V$	$0.395^{+13}_{-9}$	$0.345^{+18}_{-10}$	$0.338^{+23}_{-13}$	$0.329^{+30}_{-23}$	$0.313^{+35}_{-44}$	$0.292^{+26}_{-21}$
$A_V \times 10^1$	$0.103^{+18}_{-17}$	$0.079^{+19}_{-10}$	$0.077^{+21}_{-11}$	$0.071^{+25}_{-15}$	$0.060^{+24}_{-22}$	
$\chi^2/\text{dof}$	6.3/4	7.6/4	6.7/4	5.9/4	6.7/4	
$m_N$	$0.608^{+15}_{-8}$	$0.495^{+30}_{-8}$	$0.460^{+35}_{-11}$	$0.419^{+45}_{-17}$	$0.396^{+51}_{-39}$	$0.375^{+42}_{-17}$
$A_N \times 10^4$	$0.196^{+56}_{-25}$	$0.091^{+45}_{-13}$	$0.070^{+38}_{-12}$	$0.053^{+37}_{-12}$	$0.052^{+46}_{-21}$	
$\chi^2/\text{dof}$	1.7/4	2.2/4	2.2/4	3.1/4	5.7/4	
$m_\Delta$	$0.678^{+15}_{-12}$	$0.598^{+25}_{-15}$	$0.577^{+25}_{-22}$	$0.565^{+33}_{-33}$	$0.586^{+89}_{-62}$	$0.513^{+40}_{-31}$
$A_\Delta \times 10^3$	$0.080^{+16}_{-15}$	$0.037^{+11}_{-6}$	$0.029^{+9}_{-8}$	$0.026^{+12}_{-9}$	$0.036^{+64}_{-19}$	
$\chi^2/\text{dof}$	1.2/4	11.4/4	11.1/4	7.5/4	3.2/4	
SW (SL)						
$\kappa$	0.14144	0.14226	0.14244	0.14262	0.14280	$0.14311^{+6}_{-3}$
$m_P$	$0.304^{+6}_{-5}$	$0.216^{+7}_{-5}$	$0.194^{+7}_{-5}$	$0.169^{+8}_{-6}$	$0.136^{+13}_{-8}$	0.0
$A_P \times 10^{-1}$	$0.716^{+59}_{-66}$	$0.636^{+47}_{-46}$	$0.648^{+41}_{-45}$	$0.693^{+42}_{-50}$	$0.836^{+97}_{-98}$	
$\chi^2/\text{dof}$	6.4/4	5.0/4	5.0/4	4.7/4	3.8/4	
$m_V$	$0.398^{+9}_{-5}$	$0.349^{+13}_{-11}$	$0.338^{+16}_{-15}$	$0.325^{+21}_{-19}$	$0.310^{+39}_{-29}$	$0.299^{+20}_{-18}$
$A_V \times 10^{-1}$	$0.831^{+79}_{-59}$	$0.650^{+77}_{-67}$	$0.600^{+86}_{-73}$	$0.542^{+114}_{-83}$	$0.484^{+216}_{-120}$	
$\chi^2/\text{dof}$	2.8/4	2.1/4	2.3/4	3.0/4	4.9/4	
$m_N$	$0.609^{+13}_{-9}$	$0.503^{+11}_{-13}$	$0.474^{+13}_{-15}$	$0.447^{+15}_{-22}$	$0.408^{+26}_{-24}$	$0.383^{+19}_{-26}$
$A_N$	$0.308^{+55}_{-58}$	$0.150^{+24}_{-28}$	$0.127^{+25}_{-33}$	$0.118^{+25}_{-41}$	$0.108^{+28}_{-30}$	
$\chi^2/\text{dof}$	11.1/4	13.7/4	15.5/4	16.6/4	15.8/4	
$m_\Delta$	$0.664^{+12}_{-8}$	$0.598^{+18}_{-11}$	$0.582^{+24}_{-13}$	$0.567^{+36}_{-17}$	$0.549^{+60}_{-32}$	$0.528^{+24}_{-22}$
$A_\Delta \times 10^{-1}$	$0.143^{+17}_{-17}$	$0.094^{+20}_{-13}$	$0.085^{+24}_{-13}$	$0.078^{+30}_{-14}$	$0.071^{+41}_{-17}$	
$\chi^2/\text{dof}$	1.6/4	1.1/4	1.4/4	2.7/4	6.3/4	

Table 4: Hadron masses and amplitudes, in lattice units, for the SW action. The last column contains the values obtained by linear extrapolation to  $m_P = 0$ .

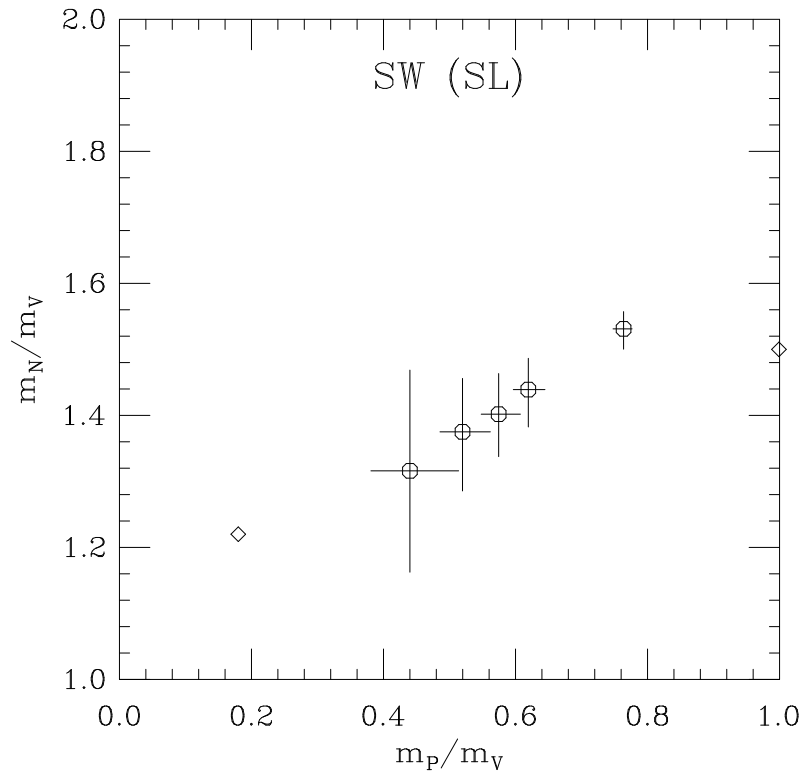


Figure 2: Edinburgh plot for the SW action using sink smearing.

physical quantity	$a^{-1}(\text{GeV})$		
	Wilson	SW (LL)	SW (SL)
$m_\rho$	$2.77^{+9}_{-23}$	$2.63^{+21}_{-22}$	$2.57^{+16}_{-16}$
$m_N$	$2.39^{+10}_{-12}$	$2.50^{+12}_{-25}$	$2.45^{+18}_{-11}$
$m_\Delta$	$2.48^{+8}_{-15}$	$2.40^{+16}_{-17}$	$2.33^{+10}_{-10}$
$(m_{K^*} - m_\rho)/(m_K^2 - m_\pi^2)$	$2.05^{+25}_{-46}$	$2.06^{+46}_{-48}$	$1.93^{+34}_{-33}$
$\sqrt{K}$	$2.73^{+5}_{-5}$		

Table 5: Scales determined from different physical quantities.

From the bootstrap analysis, we find that there are strong correlations between the pseudoscalar meson masses at different  $\kappa$  values. Figure 3 shows correlated linear fits to the data for  $m_P^2$  versus  $1/2\kappa$  for both actions, at all five  $\kappa$  values, confirming PCAC behaviour throughout the quark mass range used. The strong correlations presumably account for the remarkable linearity of our best estimates for  $m_P^2$  as functions of  $1/2\kappa$ , given the size of the statistical errors. From the chiral extrapolation, we obtain

$$\begin{aligned}
\kappa_{crit} &= 0.15328^{+7}_{-4} && (\text{Wilson}), \\
\kappa_{crit} &= 0.14313^{+7}_{-4} && (\text{SW LL}), \\
\kappa_{crit} &= 0.14311^{+6}_{-3} && (\text{SW SL}).
\end{aligned}
\tag{29}$$

The lattice scales obtained from correlated linear extrapolations of the other hadron masses to the chiral limit are presented in Table 5. For both actions, the scales derived from  $m_\rho$  agree well with the scale from the string tension, whereas the scales from the baryon masses, whilst consistent with one another, are lower, by  $2 - 3\sigma$  for the SW data and more than  $3\sigma$  for the Wilson data. We have investigated quadratic chiral extrapolations, but find that we can attach no statistical significance to any difference between the extrapolations.

The value of  $\kappa$  corresponding to the strange quark may be estimated by assuming that the pseudoscalar meson mass obeys

$$m_P^2(\kappa_1, \kappa_2) = b_P \left( \frac{1}{2\kappa_1} + \frac{1}{2\kappa_2} - \frac{1}{\kappa_{crit}} \right)
\tag{30}$$

for valence quark masses corresponding to  $\kappa_1$  and  $\kappa_2$ . We determine  $b_P$  and  $\kappa_{crit}$  from the data for degenerate valence quarks, and match  $m_P(\kappa_s, \kappa_{crit})$  to the physical kaon mass, taking the scale from  $m_\rho$ . This gives

$$\kappa_s = 0.1517^{+1}_{-3} \text{ (Wilson)}, \quad \kappa_s = 0.1418^{+2}_{-2} \text{ (SW SL)}.
\tag{31}$$

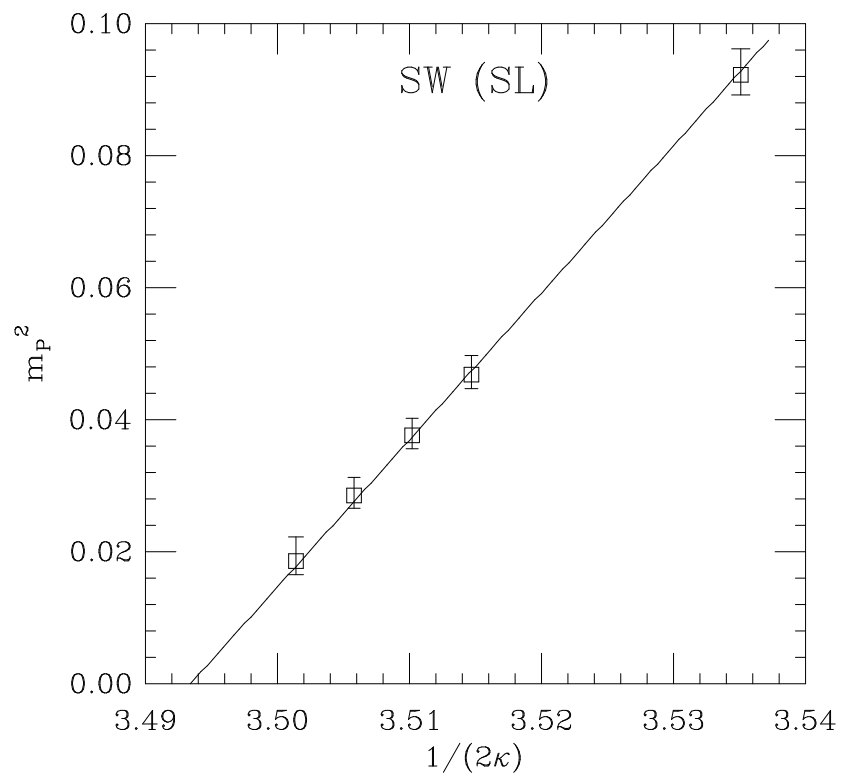
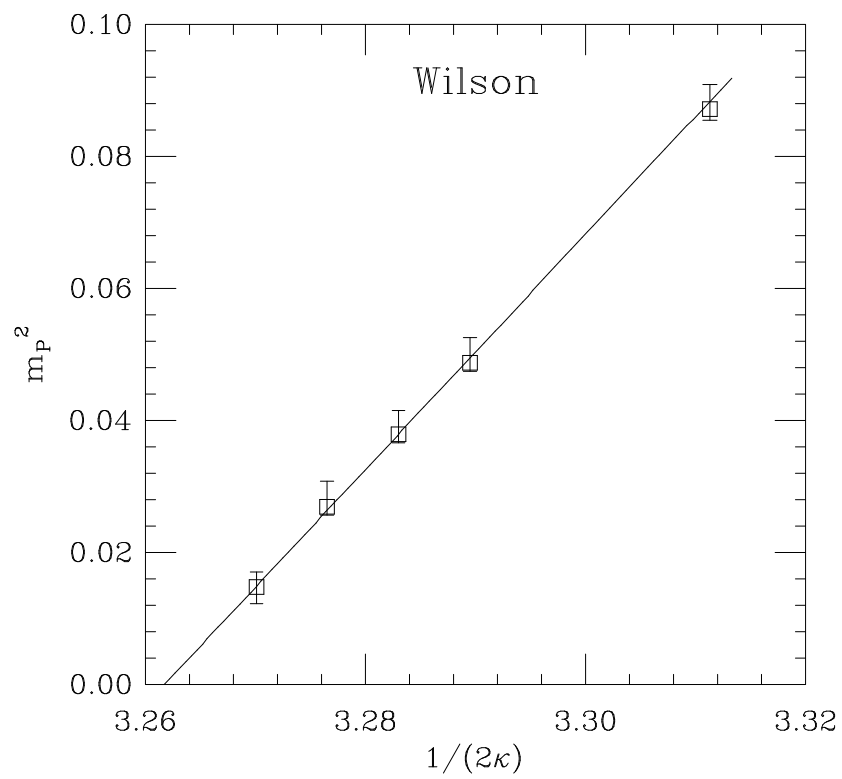


Figure 3:  $m_P^2$  versus  $1/2\kappa$ .



### 3.3 Mass Splittings

In an attempt to highlight any differences arising from use of the SW action, we present estimates for the vector-pseudoscalar meson and  $\Delta$ -nucleon mass splittings, which in QCD-inspired quark models arise from spin interactions and therefore may be corrected at  $O(a)$  by the spin term in the SW action. The suggestion that the vector-pseudoscalar mass splitting might be susceptible to lattice artefacts has been made previously by the APE collaboration in a comparative study [31] of Wilson and staggered fermion actions, albeit at stronger coupling than the present work.

Experimentally, for both light-light and heavy-light mesons,  $m_V^2 - m_P^2$  is very nearly independent of quark mass:  $0.57 \text{ GeV}^2$  ( $\rho - \pi$ ),  $0.55 \text{ GeV}^2$  ( $K^* - K$ ),  $0.55 \text{ GeV}^2$  ( $D^* - D$ ), whereas for the charmonium system  $m_{J/\psi}^2 - m_{\eta_c}^2 = 0.72 \text{ GeV}^2$ , suggesting that for systems composed of equal-mass quarks, this quantity increases slowly with quark mass. Taking the scale from the string tension, the range of pseudoscalar meson masses for which we have data is 330 MeV to 800 MeV. Thus, it is of interest to study the quark-mass dependence of our data for  $m_V^2 - m_P^2$ , with equal-mass quarks. In Figure 4, we plot the quantity  $m_V^2 - m_P^2$ , calculated directly from the bootstrap masses, versus  $m_P^2$ , for both actions. The Wilson data is consistent with previous work [32] which indicated a negative slope, inconsistent with experiment at large quark mass. The larger statistical errors in the SW data leave open the possibility of a reduced dependence on quark mass, although it appears that there is still a tendency for the hyperfine splitting to decrease with increasing quark mass. We have shown in a related study [33] that at heavier quark masses this is indeed the case; the SW estimate of the hyperfine splitting in charmonium is a factor of 1.8 larger than the Wilson estimate, although still smaller by a factor of roughly two than the experimental value. Using the string tension scale, the experimental value for light quarks corresponds to 0.075 in lattice units, consistent with the three lightest Wilson points and all the SW points.

The  $\Delta$ -nucleon mass splittings for the two actions, estimated from the bootstrap samples, are shown in Figure 5. Using the scale set by the string tension, the experimental result of 300 MeV would translate to 0.11 in lattice units, a value broadly consistent with both the Wilson and the SW data. However, the errors in both data sets are too large for this quantity to discriminate between the two actions.

It has been noted that the ratio  $(m_{K^*} - m_\rho)/(m_K^2 - m_\pi^2)$  typically gives a value for the inverse lattice spacing which is lower than that obtained using other physical quantities [34]. Assuming that the vector meson mass is linear in the quark masses, with slope  $b_V$  and intercept  $a_V$ :

$$m_V(\kappa_1, \kappa_2) = a_V + \frac{b_V}{b_P} m_P^2(\kappa_1, \kappa_2) \quad (32)$$

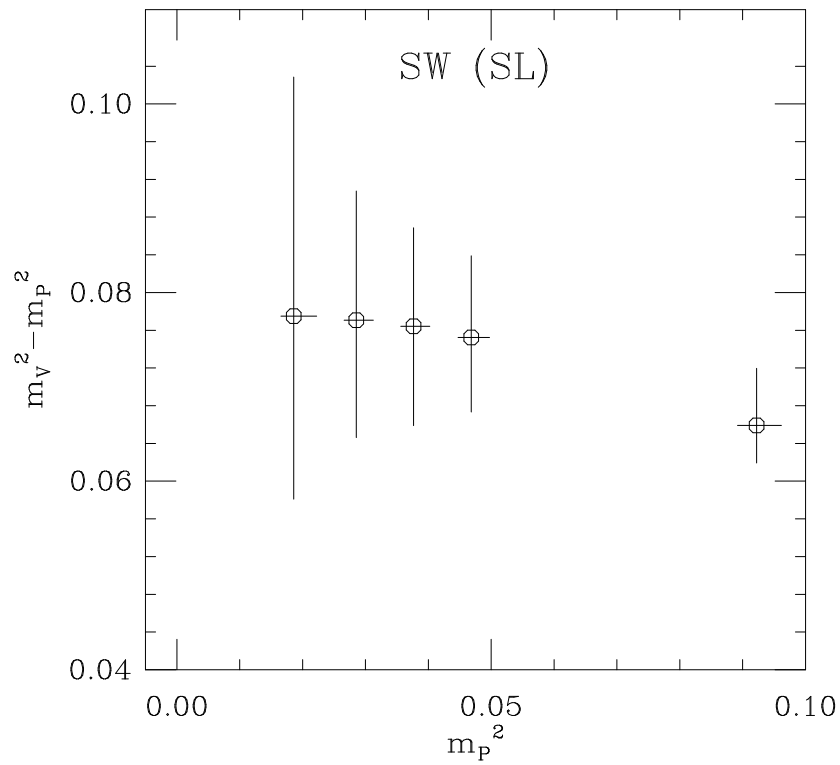
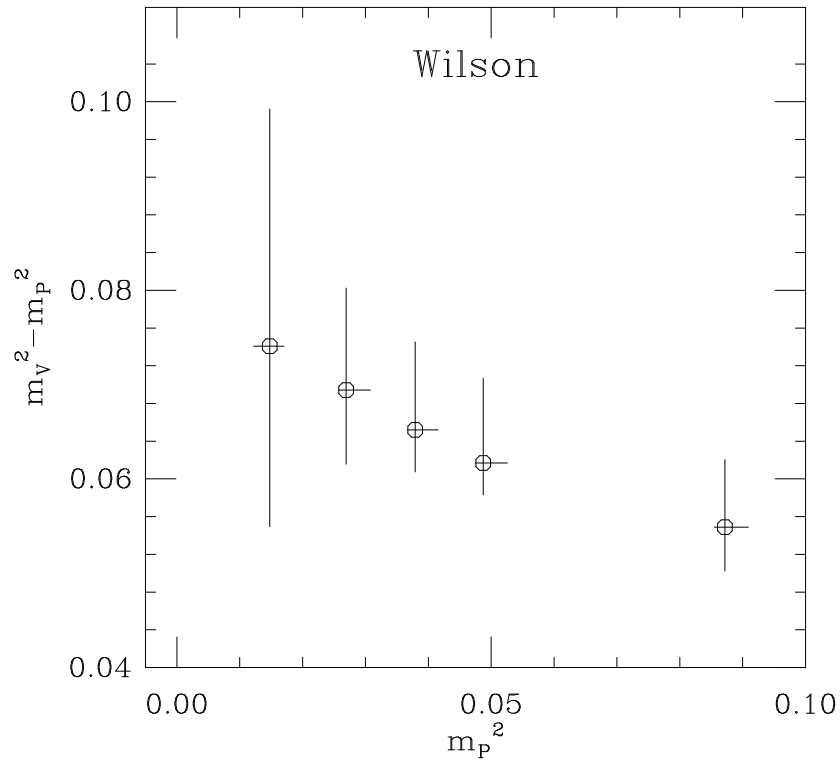


Figure 4:  $m_V^2 - m_P^2$  versus  $m_P^2$ , in lattice units.

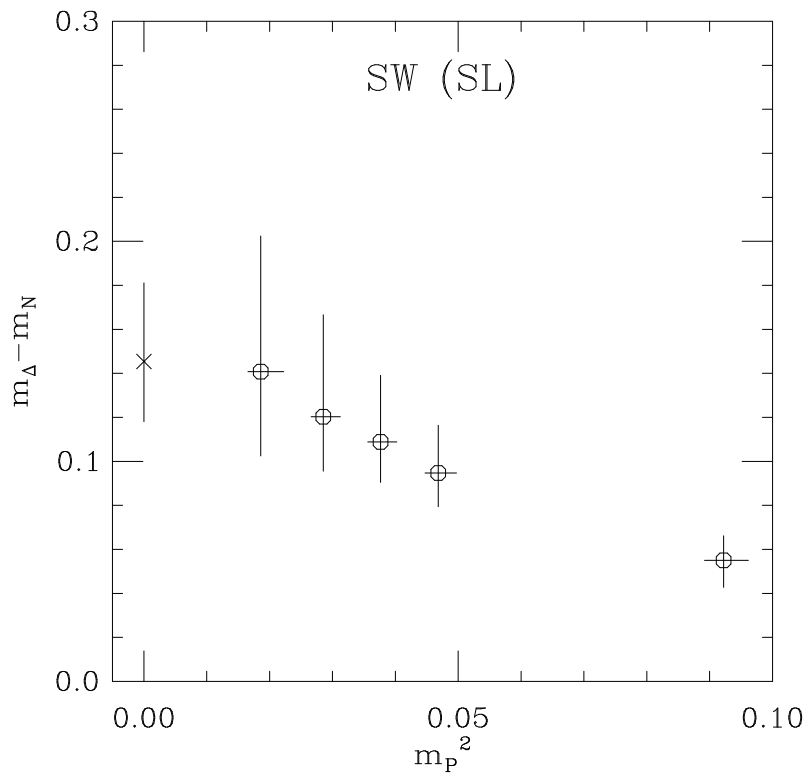
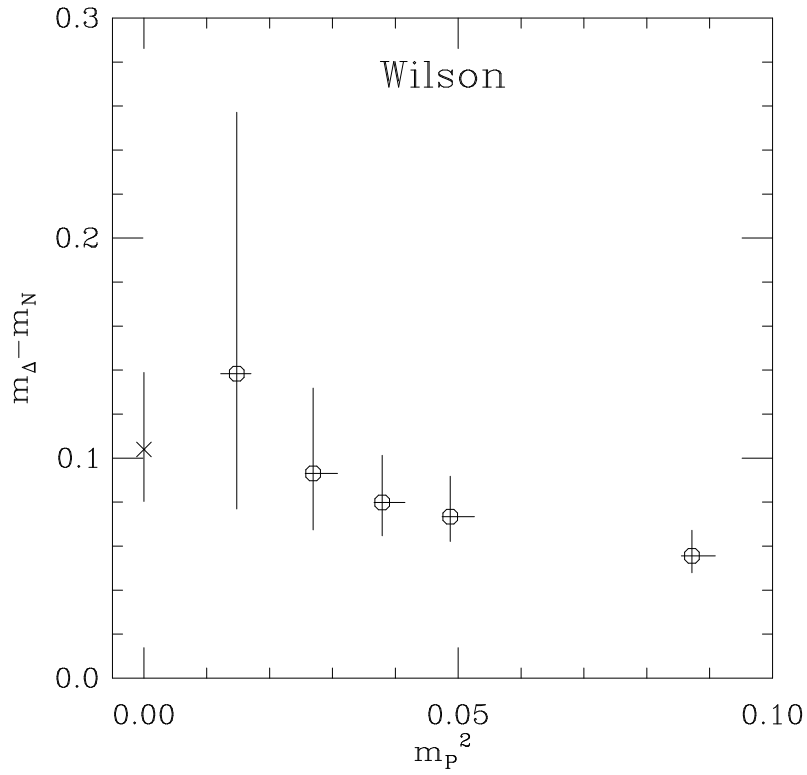


Figure 5:  $\Delta$ -nucleon mass splitting; the left-most point in each plot is obtained from the chiral extrapolation of the individual masses.

we obtain the scales given in Table 5 from

$$\frac{m_{K^*} - m_\rho}{m_K^2 - m_\pi^2} = \frac{m_V(\kappa_s, \kappa_{crit}) - m_V(\kappa_{crit}, \kappa_{crit})}{m_P^2(\kappa_s, \kappa_{crit}) - m_P^2(\kappa_{crit}, \kappa_{crit})} = \frac{b_V}{b_P}. \quad (33)$$

We find that the scales for the two actions are in good agreement with each other, but our best determinations are more than one standard deviation below the baryon scales and more than two standard deviations below the string tension scale.

## 4 Meson Decay Constants

### 4.1 Pseudoscalar Decay Constants

We determine the pseudoscalar decay constant,  $f_P$ , through the matrix element of the fourth component of the lattice axial current:

$$Z_A \langle 0 | \bar{q}(0) \gamma_4 \gamma_5 q(0) | P(p) \rangle = f_P m_P \quad (34)$$

where our normalisation is such that the physical value of  $f_\pi$  is 132 MeV. The factor  $Z_A$  is required to ensure that the lattice current obeys the correct current algebra in the continuum limit [35].

Because the signal for  $\sum_{\mathbf{x}} \langle A_4(\mathbf{x}, t) A_4^\dagger(0) \rangle$  is unacceptably noisy, for both the Wilson and SW actions, we determine  $f_P$  using the LL propagators by fitting the ratio

$$\frac{\sum_{\mathbf{x}} \langle A_4(\mathbf{x}, t) A_4^\dagger(0) \rangle}{\sum_{\mathbf{x}} \langle P(\mathbf{x}, t) P^\dagger(0) \rangle} \sim \frac{f_P^2 m_P^2}{Z_A^2 |\langle 0 | P | P \rangle|^2}. \quad (35)$$

where  $m_P$  and  $\langle 0 | P | P \rangle$  are obtained from a separate least- $\chi^2$  fit to  $\sum_{\mathbf{x}} \langle P(\mathbf{x}, t) P^\dagger(0) \rangle$ . The errors in  $f_P$  are determined by a bootstrap analysis on the whole procedure.

The measurements of  $f_P$  reported in [6] for the SW action displayed much larger errors than those for the standard Wilson action. For the SW action, we computed the correlator  $\sum_{\mathbf{x}} \langle A_4(\mathbf{x}, t) P^\dagger(0) \rangle$ , and thus we are also able to obtain  $f_P$  by fitting the ratio

$$\frac{\sum_{\mathbf{x}} \langle A_4(\mathbf{x}, t) P^\dagger(0) \rangle}{\sum_{\mathbf{x}} \langle P(\mathbf{x}, t) P^\dagger(0) \rangle} \sim \frac{f_P m_P}{Z_A \langle 0 | P | P \rangle} \tanh m_P (L_t/2 - t), \quad (36)$$

where  $m_P$  and  $\langle 0 | P | P \rangle$  are obtained from the fit to  $\sum_{\mathbf{x}} \langle P(\mathbf{x}, t) P^\dagger(0) \rangle$ .

We found that, for the light hadron sector using Wilson fermions, the use entirely of local operators provided a good determination of  $f_P$ , and the introduction of SL and SS propagators offered no improvement [29]. Therefore, we did not pursue the determination of  $f_\pi$  using the SL propagators.

Wilson using $\sum_{\mathbf{x}} \langle A_4(\mathbf{x}, t) A_4^\dagger(0) \rangle$		
$\kappa$	$(f_P)/Z_A^W$	$(f_P/m_V)/Z_A^W$
0.1510	$0.081^{+4}_{-3}$	$0.22^{+1}_{-1}$
0.1520	$0.069^{+5}_{-5}$	$0.21^{+1}_{-2}$
0.1523	$0.066^{+5}_{-9}$	$0.21^{+2}_{-3}$
0.1526	$0.065^{+5}_{-12}$	$0.21^{+2}_{-4}$
0.1529	$0.067^{+7}_{-16}$	$0.23^{+3}_{-6}$
0.15328	$0.056^{+8}_{-9}$	$0.21^{+2}_{-4}$

SW using $\sum_{\mathbf{x}} \langle A_4(\mathbf{x}, t) A_4^\dagger(0) \rangle$			SW using $\sum_{\mathbf{x}} \langle A_4(\mathbf{x}, t) P^\dagger(0) \rangle$		
$\kappa$	$(f_P)/Z_A^C$	$(f_P/m_V)/Z_A^C$	$\kappa$	$(f_P)/Z_A^C$	$(f_P/m_V)/Z_A^C$
0.14144	$0.060^{+5}_{-3}$	$0.15^{+1}_{-1}$	0.14144	$0.064^{+2}_{-2}$	$0.16^{+1}_{-1}$
0.14226	$0.048^{+7}_{-4}$	$0.14^{+2}_{-2}$	0.14226	$0.052^{+2}_{-3}$	$0.15^{+1}_{-1}$
0.14244	$0.046^{+8}_{-6}$	$0.14^{+2}_{-2}$	0.14244	$0.049^{+2}_{-3}$	$0.15^{+1}_{-2}$
0.14262	$0.046^{+8}_{-8}$	$0.14^{+3}_{-3}$	0.14262	$0.047^{+2}_{-3}$	$0.14^{+1}_{-2}$
0.14280	$0.046^{+11}_{-10}$	$0.15^{+5}_{-3}$	0.14280	$0.044^{+3}_{-5}$	$0.14^{+2}_{-2}$
0.14313	$0.037^{+12}_{-8}$	$0.13^{+4}_{-3}$	0.14313	$0.039^{+2}_{-4}$	$0.13^{+1}_{-2}$

Table 6: Values of the pseudoscalar decay constant, in lattice units, and the ratio  $f_P/m_V$ . The last row in each table contains values obtained by a linear extrapolation to the chiral limit.

In Table 6, we present the values obtained for  $f_P$  and for the dimensionless ratio  $f_P/m_V$ , using the Wilson action with the local axial current, and the SW action with the ‘improved’ axial current:

$$\bar{q}(x) \left( 1 + \frac{1}{2} \gamma \cdot \overleftarrow{D} \right) \gamma_\mu \gamma_5 \left( 1 - \frac{1}{2} \gamma \cdot \overrightarrow{D} \right) q(x). \quad (37)$$

The final row contains results for each column after linear extrapolation in  $1/\kappa$  to the chiral limit. The measurement of  $f_P$  for the SW action through the axial-pseudoscalar correlator is clearly much less noisy than that through the axial-axial correlator, and will be used in the following discussion. Our lattice results for  $f_P/m_V$  vary only slowly with quark mass, in agreement with the experimental observation that  $f_\pi/m_\rho$  (0.17) is approximately the same as  $f_K/m_{K^*}$  (0.18). The chiral extrapolation of this quantity may therefore be more reliable than that of  $f_P$  alone.

In order to determine the physical values, the lattice results given in Table 6 need to be multiplied by the appropriate renormalisation constant,  $Z_A^W$  or  $Z_A^C$ .

$$Z_A^W \simeq 1 - 0.132g^2 \quad (38)$$

in perturbation theory. If we use the bare coupling constant as the expansion parameter, then  $Z_A^W \simeq 0.87$  and we find, for the Wilson action,  $f_\pi/m_\rho = 0.18_{-3}^{+2}$ . However, reference [18] proposes the use of an ‘effective coupling’,  $g_{\text{eff}}$ , defined through

$$g_{\text{eff}}^2 = \frac{g_0^2}{\langle \frac{1}{3} \text{Tr} U_\square \rangle} \left( 1 + \frac{0.513}{4\pi} g_{\text{eff}}^2 + O(g_{\text{eff}}^4) \right). \quad (39)$$

where  $g_0$  is the bare coupling. At  $\beta = 6.2$ ,  $g_{\text{eff}}^2 \simeq 1.75g_0^2$  yielding  $Z_A^W \simeq 0.78$ , and we obtain  $f_\pi/m_\rho = 0.16_{-3}^{+2}$ .

The perturbative estimate [36] of the renormalisation constant  $Z_A^C$  is close to 1,

$$Z_A^C \simeq 1 - 0.0177g^2; \quad (40)$$

using the bare coupling leads to  $Z_A^C \simeq 0.98$ , whereas the effective coupling gives  $Z_A^C \simeq 0.97$ , yielding, for the SW action,  $f_\pi/m_\rho = 0.13_{-2}^{+1}$  in both cases. We note that the uncertainty in  $Z_A$  due to the choice of the perturbative expansion parameter is about 10% with the Wilson action and only about 1% with the SW action.

A recent non-perturbative estimate of  $Z_A^C$ , based on the use of chiral Ward identities, gave the result  $Z_A^C = 1.09(3)$ , about 10% higher than the one-loop perturbative values quoted above [37]. This result was obtained from a simulation at  $\beta = 6.0$  using a single value of the quark mass. Although it is expected that the dependence of  $Z_A^C$  on the lattice spacing and quark mass should be very mild, we feel that this expectation should be checked before the non-perturbative value is adopted in the present calculation. We note however that if the non-perturbative value of  $Z_A^C$  proves to be stable, the discrepancy between the result for  $f_\pi/m_\rho$  which we obtain using the SW action and the physical value is considerably reduced. This underlines the importance of reliable non-perturbative determinations of the renormalisation constants in order to get better estimates of the remaining lattice systematic errors, such as quenching.

Figure 6 shows  $f_P/m_V$  against  $m_P^2$  in physical units for both actions, with the lattice spacing determined from  $m_\rho$ , and  $Z_A$  computed using the effective coupling. Although the behaviour of this ratio with  $m_P^2$  for the SW action is very encouraging, there is a clear discrepancy with the physical values in the overall normalisation.

If we assume that the pseudoscalar decay constant obeys

$$f_P = a_f + b_f m_P^2(\kappa_1, \kappa_2), \quad (41)$$

where  $m_P^2(\kappa_1, \kappa_2)$  is given by Equation (30), then

$$\frac{f_K}{f_\pi} - 1 = \frac{b_f}{a_f} m_P^2(\kappa_s, \kappa_{\text{crit}}). \quad (42)$$

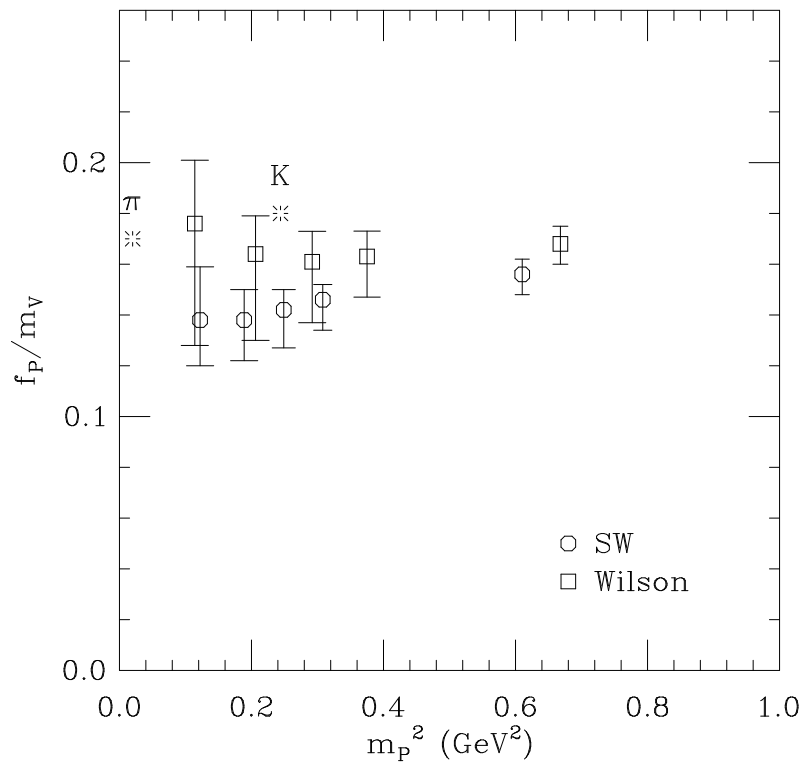


Figure 6:  $f_P/m_V$  against  $m_P^2$ , with lattice spacing determined from  $m_\rho$ , and  $Z_A$  computed using the effective coupling.

Wilson		SW	
$\kappa$	$1/(Z_V^W f_V)$	$\kappa$	$1/(Z_V^C f_V)$
0.1510	$0.40^{+1}_{-1}$	0.14144	$0.33^{+1}_{-2}$
0.1520	$0.43^{+1}_{-1}$	0.14226	$0.36^{+2}_{-1}$
0.1523	$0.44^{+1}_{-1}$	0.14244	$0.36^{+2}_{-1}$
0.1526	$0.45^{+1}_{-1}$	0.14262	$0.37^{+2}_{-1}$
0.1529	$0.47^{+2}_{-1}$	0.14280	$0.36^{+2}_{-1}$
0.15328	$0.47^{+2}_{-1}$	0.14313	$0.38^{+3}_{-1}$

Table 7: Values of the vector meson decay constant. The last row contains values obtained by a linear extrapolation to the chiral limit.

We take  $a_f$  and  $b_f$  from the fit to the data in Table 6, and using  $\kappa_s$  values from Equation (31) we obtain

$$\frac{f_K}{f_\pi} - 1 = 0.16^{+10}_{-5} \quad (\text{Wilson}), \quad \frac{f_K}{f_\pi} - 1 = 0.25^{+7}_{-4} \quad (\text{SW}), \quad (43)$$

compared to the experimental value of 0.22. Note that the ratio is less sensitive to uncertainties both in the renormalisation of the axial current and in the scale.

## 4.2 Vector Meson Decay Constant

The vector meson decay constant is defined by the relation

$$Z_V \langle 0 | \bar{q}(0) \gamma_\mu q(0) | V \rangle = \frac{m_V^2}{f_V} \epsilon_\mu \quad (44)$$

where  $\epsilon_\mu$  is the polarisation vector of the meson and  $Z_V$  is the renormalisation constant for the lattice vector current [35]. We determine  $f_V$ , using the LL propagators, by fitting to

$$\sum_{j=1}^3 \sum_{\mathbf{x}} \langle V_j(\mathbf{x}, t) V_j^\dagger(0) \rangle \sim \frac{3m_V^3}{2Z_V^2 f_V^2} e^{m_V L_t/2} \cosh m_V (L_t/2 - t). \quad (45)$$

For the Wilson action we use the local current and for the SW action we use the improved local current. We obtain the values shown in Table 7. We extrapolate linearly in  $1/\kappa$  to obtain the values at the chiral limit.

The renormalisation constants corresponding to our choice of the lattice vector currents are given in perturbation theory by [36]

$$Z_V^W \simeq 1 - 0.17g^2 \quad (46)$$

$$Z_V^C \simeq 1 - 0.10g^2. \quad (47)$$

The one-loop perturbative correction, although smaller for the SW action than for the Wilson action, is still substantial and it introduces a significant uncertainty in  $f_V$  due to the



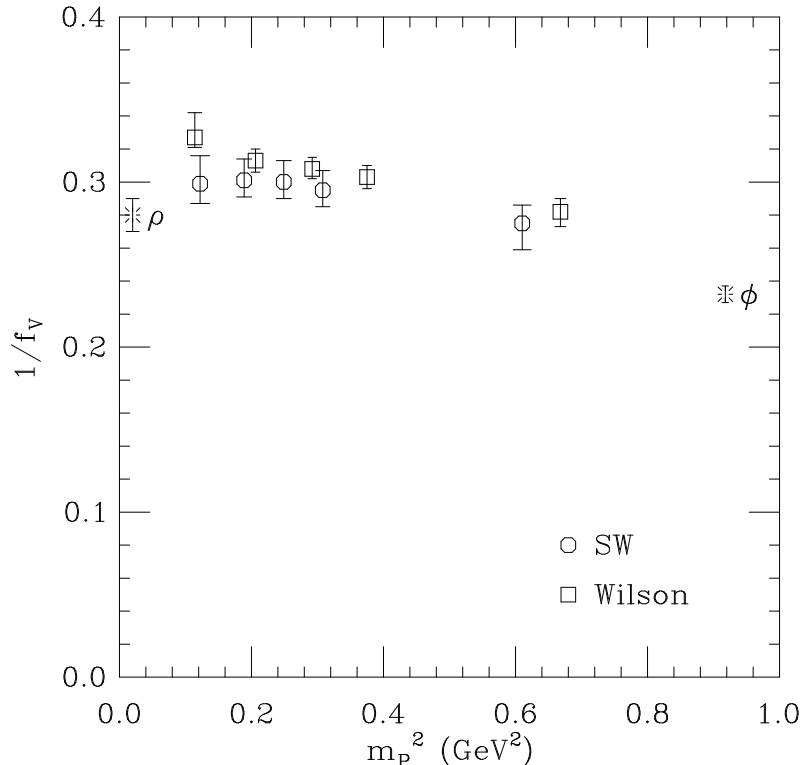


Figure 7:  $1/f_V$  against  $m_P^2$ , with lattice spacing determined from  $m_\rho$ , and  $Z_V$  computed using the effective coupling.

uncertainty in the value of the expansion parameter. Recent non-perturbative estimates of  $Z_V^C$  at  $\beta = 6.0$  [37] give a value which agrees well with that obtained by using the effective coupling defined in Equation (39). Since the non-perturbative values of  $Z_V$  for the two actions are not yet known at  $\beta = 6.2$ , we use the effective coupling in the perturbative expressions for comparison with experiment, i.e.,

$$Z_V^W \simeq 0.71 \quad (48)$$

$$Z_V^C \simeq 0.83. \quad (49)$$

We note that the perturbative uncertainty would be removed entirely by use of the conserved vector current.

Our results for  $f_V$  are compared with experimental values in Figure 7. We do not know which pseudoscalar meson mass to associate with the experimental value of  $f_\phi$  in this plot. For the purpose of illustration, we take the pseudoscalar meson mass to be the mass of the  $\eta'$ . Despite this uncertainty and the presumably small residual uncertainty in the overall normalisation, we find the agreement with experiment encouraging. In the chiral limit we

obtain

$$1/f_\rho = 0.33^{+1}_{-1} \quad (\text{Wilson}) \quad (50)$$

$$1/f_\rho = 0.31^{+2}_{-1} \quad (\text{SW}) \quad (51)$$

compared to the physical value of  $1/f_\rho$  of 0.28(1). Again this discussion points to the need for a non-perturbative determination of the current renormalisation constants.

## 5 Conclusions

Significant differences have already been reported between the mass splittings obtained using the SW and Wilson fermion actions for systems involving heavy quarks [33, 38]. To obtain a complete picture of the effects of the  $O(a)$ -improvement proposed by Sheikholeslami and Wohlert, it is necessary also to study the light quark sector. Our main conclusion is that at  $\beta = 6.2$ , for pseudoscalar meson masses in the range 330–800 MeV, there is no statistically significant difference between the results for the hadron spectrum or decay constants obtained with the two actions. This supports the validity of results obtained for light hadrons with the Wilson action over the last few years.

We find that the scales obtained from the meson sector are consistent with that from the string tension, but there is evidence of inconsistent scales from the baryon sector and from the ratio  $(m_{K^*} - m_\rho)/(m_K^2 - m_\pi^2)$ .

Our calculation of  $f_P/m_V$  with the SW action yields a result whose dependence on the quark mass is consistent with experiment, but whose magnitude is significantly smaller. There is a small residual uncertainty in the calculated values, which could be removed by a non-perturbative determination of the axial vector current renormalisation constant. It seems likely that this will not account entirely for the discrepancy and may signal the effect of quenching. Our results for  $f_\rho$  and  $f_\phi$  are broadly in agreement with experiment.

We believe that this comparative study has established the viability of the SW formulation of quenched lattice QCD, with no significant disadvantages for light hadrons, laying the foundation for its use in the study of heavy-quark systems where discretisation errors are more serious.

## Acknowledgements

This research is supported by the UK Science and Engineering Research Council under grants GR/G 32779, GR/H 49191, GR/H 53624 and GR/H 01069, by the University of Edinburgh and by Meiko Limited. The SERC is acknowledged for its support of CTS through the

award of a Senior Fellowship and of ADS through the award of a Personal Fellowship. We are grateful to Edinburgh University Computing Service for use of its DAP 608 for some of the analysis and, in particular, to Mike Brown for his tireless efforts in maintaining service on the Meiko i860 Computing Surface.

## References

- [1] M. Lüscher & P. Weisz, *Commun. Math. Phys.* 97 (1985) 59.
- [2] G. Heatlie, C.T. Sachrajda, G. Martinelli, C. Pittori & G.C. Rossi, *Nucl. Phys.* B352 (1991) 266.
- [3] K. Symanzik, *in* *Mathematical Problems in Theoretical Physics*, ed. R. Schrader, R. Seiler & D.A. Uhlenbrock, *Springer Lecture Notes in Physics*, vol. 153 (1982) 47.
- [4] W. Wetzel, *Phys. Lett.* B136 (1984) 407.
- [5] B. Sheikholeslami & R. Wohlert, *Nucl. Phys.* B259 (1985) 572.
- [6] UKQCD Collaboration, C.R. Allton et al., *Phys. Lett.* B284 (1992) 377.
- [7] K.C. Bowler, *Phys. Rep.* **207** (1991) 261.
- [8] K.C. Bowler, *The UK Grand Challenge Projects: Large-Scale Scientific Computations on a Parallel Supercomputer*, Proceedings of COMETT Seminar on Industrial Applications of Parallel Computers, Graz, Austria (1992).
- [9] S.P. Booth, *Parallel Computing in UKQCD*, Proceedings of CHEP92, CERN (1992).
- [10] M. Creutz, *Phys. Rev.* D36 (1987) 2394; F.R. Brown & T.J. Woch, *Phys. Rev. Lett.* 58 (1987) 2394.
- [11] N. Cabibbo & E. Marinari, *Phys. Lett.* B119 (1982) 387.
- [12] G. Marsaglia, A. Zaman & W.W. Tsang, *Stat. Probabil. Lett.* 9 (1990) 35.
- [13] M. Teper, *Phys. Lett.* B183 (1987) 345.
- [14] M. Albanese et al., *Phys. Lett.* B192 (1987) 163.
- [15] S. Perantonis & C. Michael, *Nucl. Phys.* B 347 (1990) 854.
- [16] C. Michael & M. Teper, *Nucl. Phys.* B 314 (1989) 347.
- [17] G.S. Bali & K. Schilling, *Phys. Rev.* D46 (1992) 2636.

- [18] G.P. Lepage & P.B. Mackenzie, Nucl. Phys. B (Proc. Suppl.) 20 (1991) 173; *On the viability of lattice perturbation theory*, Fermilab preprint FERMILAB-PUB-91-355-T-REV, September 1992.
- [19] UKQCD Collaboration, S.P. Booth et al., Phys. Lett. B294 (1992) 385.
- [20] Y. Oyanagi, Comp. Phys. Comm. 42 (1986) 333
- [21] G. M. Hockney, Nucl. Phys. B (Proc. Suppl.) 17 (1990) 301
- [22] A.D. Simpson, *Algorithms for lattice QCD*, Ph.D. thesis, University of Edinburgh (1991).
- [23] G. Martinelli, C.T. Sachrajda & A. Vladikas, Nucl. Phys. B358 (1992) 212.
- [24] G. Martinelli, C.T. Sachrajda, G. Salina & A. Vladikas, Nucl. Phys. B378 (1992) 591.
- [25] S. Güsken et al., Nucl. Phys. B (Proc. Suppl.) 17 (1990) 301.
- [26] D. Daniel, R. Gupta, G.W. Kilcup, A. Patel and S. Sharpe, Phys. Rev. D46 (1992) 3130.
- [27] R. D. Kenway, in Proceedings of XII International Conference on HEP, Leipzig (1984) 51, eds. A. Meyer and E. Wieczorek.
- [28] A. Billoire, E. Marinari, and G. Parisi, Phys. Lett. 162B (1985) 160.
- [29] UKQCD Collaboration, C.R. Allton et al., Phys. Rev. D47 (1993) 5128.
- [30] M.-C. Chu, M. Lissia & J.W. Negele, Nucl. Phys. B360 (1991) 31.
- [31] The APE Collaboration: S. Cabasino et al., Phys. Lett. B258 (1991) 195.
- [32] C.R. Allton, M. Bochicchio, D.B. Carpenter, G. Martinelli & C.T. Sachrajda, Nucl. Phys. B372 (1992) 403.
- [33] UKQCD Collaboration, C.R. Allton et al., Phys. Lett. B292 (1992) 408.
- [34] L. Maiani & G. Martinelli, Phys. Lett. B178 (1986) 265.
- [35] M. Bochicchio, L. Maiani, G. Martinelli, G. Rossi & M. Testa, Nucl. Phys. B262 (1985) 331.
- [36] A. Borrelli, C. Pittori, R. Frezzotti & E. Gabrielli, *New improved operators: a convenient redefinition*, CERN preprint TH.6587/92 (1992).
- [37] C.T. Sachrajda, Nucl. Phys. B (Proc. Suppl.) 30 (1993) 20.
- [38] A.X. El-Khadra, Nucl. Phys. B (Proc. Suppl.) 26 (1992) 372.